1

2

3

# The Central Role of the Tail in Switching Off Myosin II in Cells

5

6

7    Shixin Yang[1]*, Kyoung Hwan Lee[1a]*, John L. Woodhead[1],

8    Osamu Sato[2], Mitsuo Ikebe[2] and Roger Craig[1†]

9

10

11

12    [1] Division of Cell Biology and Imaging, Department of Radiology, University of Massachusetts
13    Medical School, Worcester MA 01655, USA

14    [2] Department of Cellular and Molecular Biology, University of Texas Health Science Center at
15    Tyler, Tyler, TX 75708, USA

16    [a] Current address: Massachusetts Facility for High-Resolution Electron Cryo-microscopy,
17    University of Massachusetts Medical School, Worcester MA 01655, USA

18    * Contributed equally

19    [†] To whom correspondence should be addressed:

20    roger.craig@umassmed.edu.

21    Ph. 508 856 2474

22

23 **Abstract**

24 Myosin II is a motor protein playing an essential role in cell motility. The molecule can exist as a
25 polymer that pulls on actin to generate motion, or as an inactive monomer with a compact
26 structure, in which its tail is folded and its two heads interact with each other. This conformation
27 functions in cells as an energy-conserving storage and transport molecule. The mechanism of
28 inhibition is not fully understood. We have carried out a 3D reconstruction of the switched-off form
29 revealing for the first time multiple interactions between the tail and the two heads that trap ATP
30 hydrolysis products, block actin binding, obstruct head phosphorylation, and prevent filament
31 formation. Blocking these essential features of myosin function can explain the high degree of
32 inhibition of the folded form of myosin, serving its energy-conserving, storage function in cells. The
33 structure also suggests a mechanism for unfolding when activated by phosphorylation.

34

## Introduction

Myosin II is a motor protein that, together with actin filaments, generates mechanical force and motion using the chemical energy of ATP hydrolysis [4]. In muscle, myosin II is responsible for shortening and force production, while in nonmuscle cells it is essential in cell adhesion and division, intracellular transport and cell migration [5]. The myosin II molecule is a hexamer composed of two heavy chains, two essential light chains (ELC) and two regulatory light chains (RLC). The light chains and the N-terminal halves of the heavy chains form two globular heads, containing ATP- and actin-binding sites, while the heavy chain C-terminal halves form an α-helical coiled-coil tail extending from the heads. The tails self-associate to form the backbone of thick filaments, which are the functional form of myosin II in muscle and cell motility. Mutations in the heads and tail impair myosin function and cause muscle disease [6, 7]. Myosin II molecules can exist in two different conformations, 6S and 10S, named for their sedimentation coefficients [8]. 10S molecules have a compact structure [2, 9-12], in which the tail is folded into three segments of similar length, and the heads are bent back on the tail and interact with each other (Fig. 1). This folded conformation traps the products of ATP hydrolysis, causing strong inhibition of ATPase
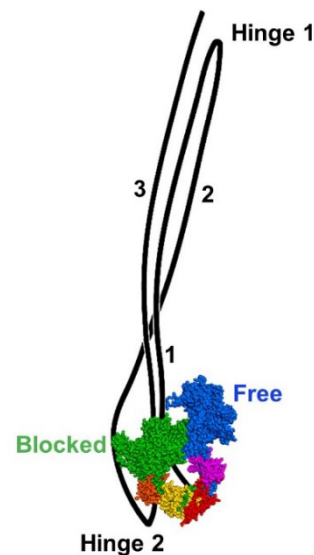


**Figure 1. Model of 10S myosin.** Blocked head consists of heavy chain (green), ELC (orange) and RLC (yellow). Free head shows heavy chain (blue), ELC (magenta) and RLC (red). The tail is folded into three segments: segment 1 (= subfragment 2), originating from the heads and ending at hinge 1; segment 2, starting at hinge 1 and ending at hinge 2; and segment 3, starting at hinge 2 and ending at the tip of the tail.

activity [13], and inhibiting assembly into thick filaments. Phosphorylation of the RLC in 10S molecules favors unfolding to the 6S form [10, 14, 15], in which ATPase activity is switched on [16] and the tail has an extended conformation, favoring filament assembly.

The inhibited, 10S molecule plays a fundamental role in nonmuscle cells, where it functions as an energy-conserving, storage form of myosin, and provides assembly units for thick filament formation when and where contractile activity is required [14]. Its compact conformation would facilitate rapid transport to the sites of filament assembly and thus motility. In smooth muscle, 10S myosin may also provide a pool of inactive monomers, which can unfold and augment myosin filament length or number when smooth muscle is activated [17-19]. In striated muscles, myosin is almost exclusively filamentous, but there is nevertheless a small concentration of 10S molecules,

3

60  whose compact form has been proposed to facilitate transport to sites of filament assembly during
61  muscle development and turnover of myosin filaments [20-22].

62  A unique structural feature of 10S myosin is an asymmetric interaction between its two heads (the
63  interacting-heads motif, or IHM), which inhibits their activity [1]. Head-head interaction was first
64  observed in two-dimensional (2D) crystals of smooth muscle heavy meromyosin in the switched-off
65  state (RLCs dephosphorylated) [1], and later confirmed by electron microscopy (EM) and 2D
66  classification of single myosin II molecules [9]. Inhibition was suggested to occur by different
67  mechanisms in the two heads. In one head ("blocked"), actin-binding is hindered by proximity of
68  the other head ("free") to its actin-binding site. In contrast, ATPase activity of the free head is
69  inhibited through stabilization of its converter domain, which interacts with the blocked head [1].
70  Three-dimensional (3D) reconstruction of thick filaments subsequently showed that 6S myosin,
71  when polymerized into thick filaments, has a similar head-head interaction to that in folded, 10S
72  molecules [23]. The IHM in thick filaments may underlie the super-relaxed state of muscle [24], in
73  which myosin activity is highly inhibited, thus serving as an important energy-conserving
74  mechanism for striated muscle.

75  The IHM structure has been compared in a variety of evolutionarily diverse species. EM and 2D
76  image classification of negatively stained molecules shows that the compact, folded form of 10S
77  myosin has been conserved since the origin of animals: head-head interactions in the IHM appear
78  similar in all species studied [2, 25, 26]. Similarly, the IHM first observed in thick filaments in cryo-
79  EM studies of tarantula muscle [23] has been confirmed in thick filaments from a variety of
80  vertebrate and invertebrate species [27-30]. The high level of conservation of the IHM in isolated
81  molecules and in thick filaments over hundreds of millions of years implies that it is a fundamental
82  structure, critical to the function of muscle and nonmuscle cells [2, 25, 26].

83  While the inhibitory interactions between the heads in the IHM are similar in thick filaments and
84  10S molecules, there are likely to be critical additional interactions with the folded tail that account
85  for the order of magnitude greater inhibition of 10S molecules compared with filaments [21, 31].
86  However, it is not known what these interactions might be, as no 3D reconstruction of the entire
87  molecule has been reported. The interactions between the myosin heads in 10S myosin were well
88  defined in studies of 2D crystals [32], but the tail was poorly visualized and the 3D reconstruction
89  provided no insights into its potential role in regulation. The tail was clearly delineated in 2D class
90  averages of isolated 10S molecules, but its course in three dimensions was not studied [9]. Here
91  we present a 3D reconstruction of 10S myosin molecules using single particle analysis. The
92  reconstruction clearly reveals the 3D course of the tail as it wraps around the heads, showing
93  evidence for interaction with the heads at eight sites, which appear to inhibit actin-binding, ATPase
94  activity, RLC phosphorylation and filament assembly by novel mechanisms. The results provide
95  new insights into how the cell conserves energy, by a total shutdown of myosin II activity in its
96  compact, storage form.

97  **Results**

98  **2D class averages of 10S myosin**

99  Turkey gizzard smooth muscle myosin at physiological ionic strength (0.15 M NaAc) in the
100  presence of ATP was observed by negative staining with 1% uranyl acetate, a technique providing
101  key insights into protein domain structures and interactions [33, 34]. The compact, folded (10S)
102  conformation dominated the EM images, with a small number of antiparallel 10S dimers, displaying
103  a dumbbell-shaped structure (Fig. 2A) and very few extended (6S) molecules. Only 10S monomers

104    were chosen for image processing. The tail in these molecules was folded into 3 segments, and
105    wrapped around the heads, as previously described [9]. The heads showed different apparent
106    shapes and sizes, corresponding to different orientations of the molecules on the EM grid (Figs. 2
107    B-E, S1). Compared to the relatively rigid arrangement of the interacting heads, the tail was quite
108    flexible where it extended away from the heads. In this region, segments 1, 2 and 3 (Fig. 1) run
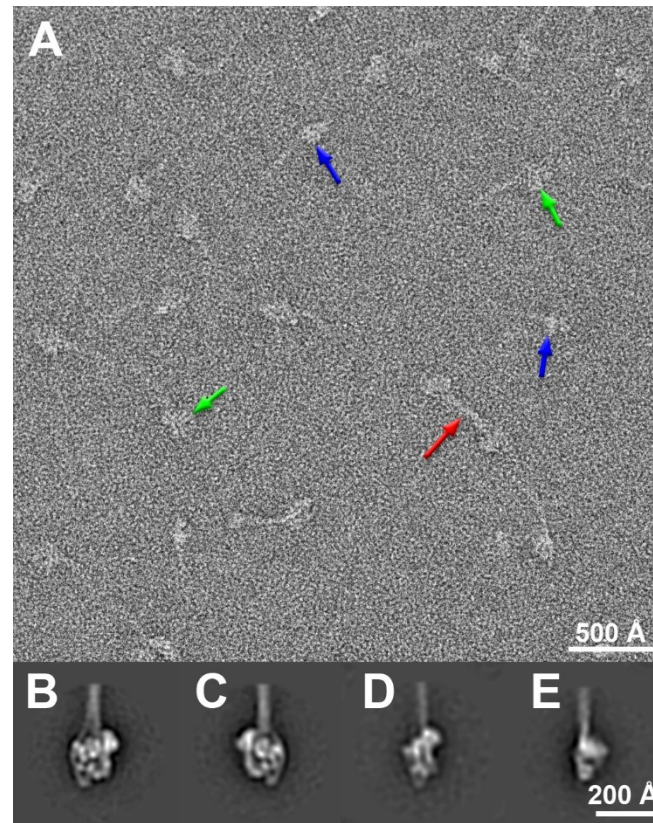


**Figure 2. Negatively stained 10S smooth muscle myosin molecules.** A. Two types of structure are visible: monomers, in front and side views (green and blue arrows, respectively), and occasional dimers (red arrow). B-D. 2D class averages of right and left views (B and C respectively [2]); (D), partially rotated view; and (E), side-view (see also Fig. S1).

109    closely together, and this combined 3-segment rod bends within a range of ~ 60º from its point of
110    emergence from the heads, as previously described [9]. Typical 2D class averages of the
111    interacting heads and the proximal portion of the 3-segment tail are shown in Figs. 2 B-E and S1.
112    The asymmetric architecture of the blocked and free heads was consistent with the results of
113    previous 2D classification analysis [2, 9, 25, 35]. Mirrored class averages, where molecules lie on
114    the grid facing down or up, were observed as previously reported [35] (Fig. S1). The class
115    averages showed that the myosin molecules typically lie parallel to the grid surface; the different
116    orientations about their long axis enabled us to analyze the 3D structure of the molecules using
117    single particle analysis.

118    **3D reconstruction**

119    An initial 3D structure of the folded molecule was computed using the random conical tilt method
120    [36], in which images are recorded at 0º and 50º tilts. This model was then used for projection

121    matching to determine the final single particle reconstruction (EMDB accession code EMD-20084).
122    Computing the initial structure *ab initio* excludes potential model bias in the final reconstruction.
123    The latter had a moderate resolution (25 Å; Fig. S2) due significantly to the flexibility of the
124    molecule [9].

125    The head region of the reconstruction has the appearance of a flat disk, with an irregular polygonal
126    "front" view (as viewed in Fig. 3A, D; Movie 1), enclosing a central hole, and a narrow side view
127    (Fig. 3C, F, Movie 1), similar to the motifs seen in the 2D crystals of HMM and myosin [1, 32] and
128    in thick filaments [23]. The atomic model of the interacting-heads structure computed from cryo-
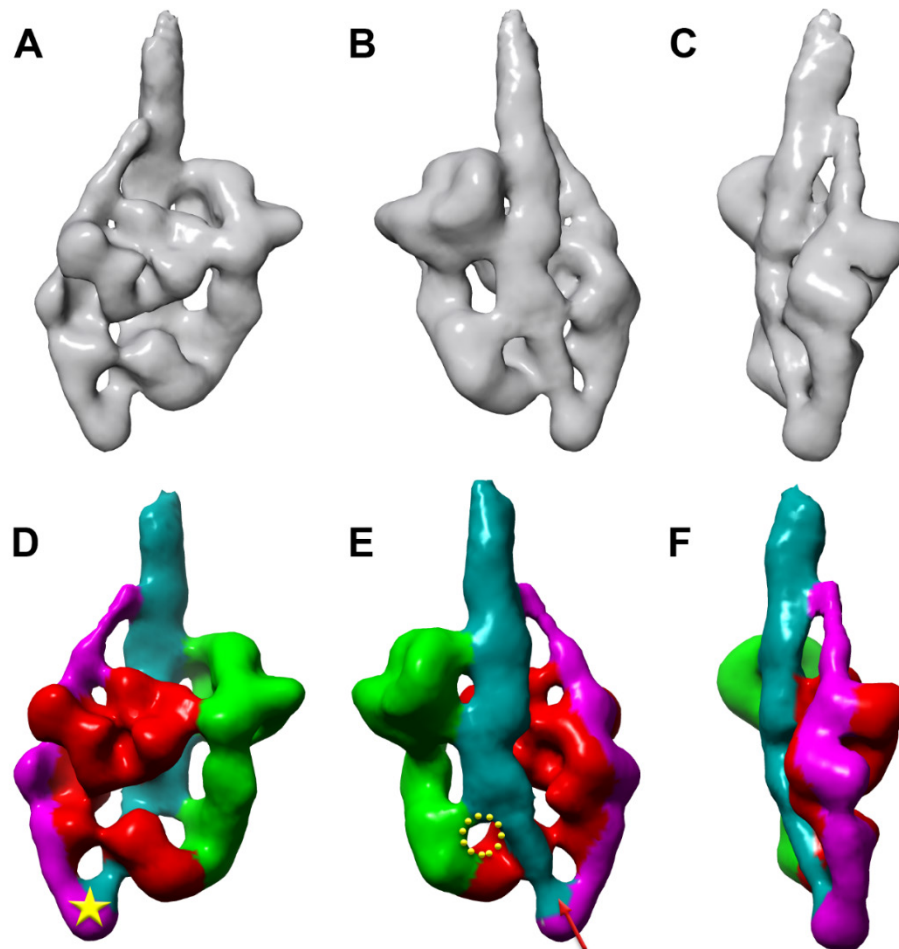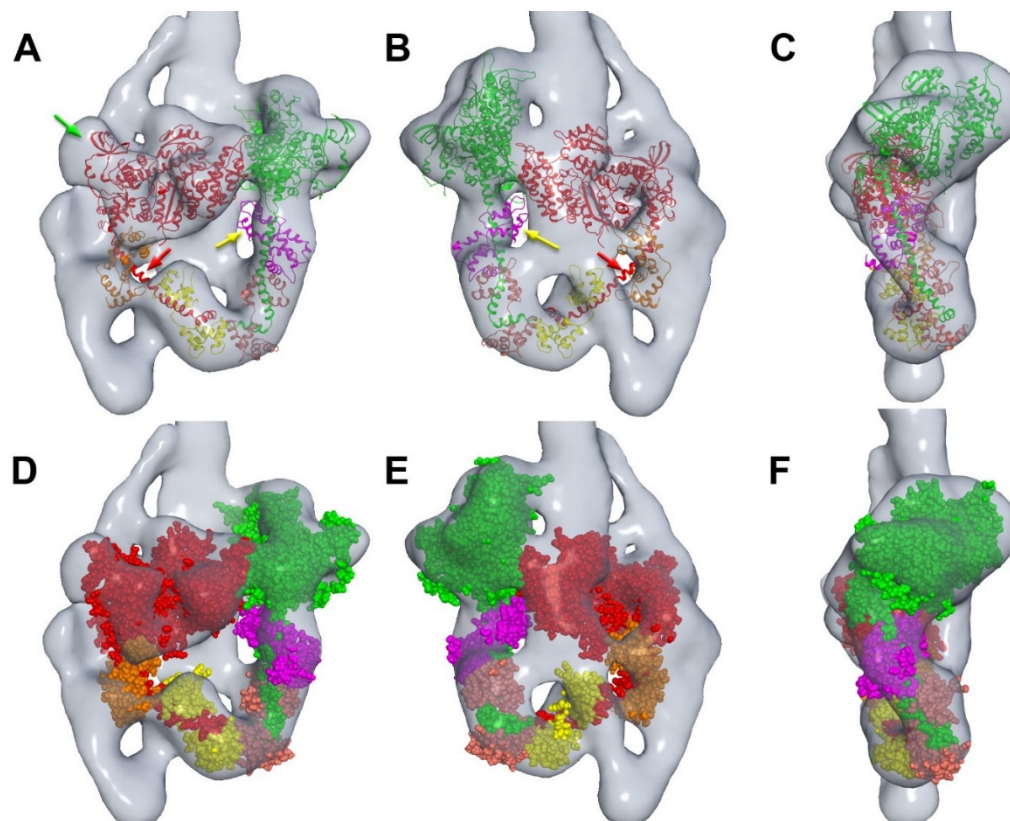


**Fig. 3. 3D reconstruction of 10S smooth muscle myosin (EMDB accession code EMD-20084).** (A), (B) and (C) are front, back and side views, respectively. (D), (E) and (F) correspond to (A), (B) and (C), with colors indicating different components of the structure. Blocked head is red; free head, green; segments 1 and 3, cyan; segment 2, magenta. In (E), yellow circle indicates putative location of missing segment 1 density (see Fig. S3); red arrow, start of segment 3. Yellow star in (D) indicates the second hinge point.

129    imaged smooth muscle HMM 2D crystals (PDB-1I84) [1] docked well into the reconstruction using
130    rigid-body fitting (Fig. 4, Movie 2), confirming this similarity. This was clear in both front- and side-
131    views (Fig. 4D, F). The fit implies excellent preservation of the IHM in negatively stained single

132    molecules (*cf.* [33]), without significant flattening, and enables us to interpret head structure and
133    interactions at higher resolution (<7 Å) than the reconstruction itself [37].

134    The reconstruction also reveals, for the first time, the course of the folded tail as it wraps around
135    the heads – a feature that was mostly missing from the only previous reconstruction of 10S myosin
136    [32]. Only a small portion of the folded tail (~150 Å) extending as three merged segments above
137    the heads was included in the reconstruction, due to flexibility of the distal region. However, the



**Figure 4. Docking of atomic model of the IHM into the reconstruction.** The 2D crystal model of smooth muscle myosin (1i84; [1]) was used in the fitting. Molecular dynamics flexible fitting was not used, due to the low resolution. (A), (B) and (C) are front, back and side views, respectively, docked with ribbon representation of the atomic model. (D)-(F) correspond to (A)-(C), but with space-filling model. The atomic model fits well into the reconstruction in all views, except for the narrow part of the lever arm in the blocked head (red arrow) and part of the ELC in the free head (yellow arrow). Unfilled densities mostly represent portions of the three segments of the tail, for which there is no atomic model. There is also some unfilled density in the blocked head (green arrow) that would be filled by repositioning the flexibly-connected SH3 domain (not done with the rigid-body docking procedure; see Methods). In a previous study, molecular dynamics flexible fitting of cryo-imaged tarantula thick filaments demonstrated this point [3]. Note: (C) and (F) rotated in opposite direction from (C) and (F) in Fig. 3.

138    essential part of the tail that interacts with the heads was included. Three segments of the tail
139    could be identified in this region (Fig. 3). Strikingly, all three appear to bind to the heads: segment
140    2 along the left side of the blocked head (Figs. 1, 3A, D), and segments 1 and 3 on the back side
141    of both heads (Fig. 3B, E, Movie 1). Segment 1 (subfragment 2 of the tail) would be expected to
142    start at the merge point of the lever arms of the blocked and free heads (blue ribbon, Fig. S3).
143    However, there was missing density for this initial portion of subfragment 2 in the reconstruction
144    (circle, Figs. 3E, S3), a known issue for this very flexible region of the tail [28, 38]; more density

7

145 becomes visible at low contour cutoff (Fig. S4). The first visible part of segment 1 density was
146 assumed to occur where the tail density (cyan) widens, as segment 1 joins segment 3 (above the
147 circle, Fig. 3E). Segment 1 then runs next to segment 3 across the blocked head (in a region now
148 known as the mesa [39]) towards the top, where segments 1 and 3 merge with segment 2 (Fig. 3D,
149 E). Segment 2 (magenta in Fig. 3) branches from the merged segments near the top and wraps
150 around the blocked head. The end of this segment and the starting point of segment 3 form the
151 second hinge point of the tail (Figs. 1, 3D), thought to occur at Glu1535 [9]. This region of density
152 (marked with a star in Fig. 3D) is unique to 10S myosin, and not found in HMM (lacking segments
153 2 and 3) or thick filaments (where the tail is unfolded). Segment 3 (red arrow in Fig. 3E) starts from
154 the hinge point, then runs, merged with segment 1, over the back of the blocked head (Fig. 3D, E)
155 to the top of the IHM where they join segment 2. This arrangement of segments 1 and 3 on the
156 same side of the IHM (Figs. 3, 5) would allow for rapid opening of the molecule upon activation. An
157 alternative arrangement, consistent with 2D projection images (Figs. 2, S1; [9]), but not with the 3D
158 structure, would have segments 1 and 3 on opposite sides, sandwiching the blocked head and
159 restricting opening of the IHM (*cf.* [9]).

160 **Intramolecular interactions within 10S smooth muscle myosin molecules**

161 The 3D reconstruction establishes key interactions occurring within the 10S myosin molecules
162 (summarized in Table 1). Three types of interaction were found: head-head, head-tail, and tail-

163

164 **Table 1: Summary of IHM interactions**

| Interaction | Interacting components | Molecule/filament | Cartoon |
|---|---|---|---|
| BF | Blocked head, free head | 10S, filament | |
| TB1 | Segments 1 and 2, blocked head mesa | 10S, filament | |
| TB2 | Segment 2, blocked head SH3 | 10S, filament | |
| TB3 | Segment 2, blocked head converter | 10S, filament | |
| TB4 | Segment 2, blocked head ELC | 10S | |
| TB5 | Segment 3, blocked head RLC | 10S | |
| TF1 | Segment 1 or 3, free head actin-binding loop | 10S, filament | |
| TF2 | Segment 1 or 3, free head ATPase loop 5 | 10S | |
| TF3 | Segment 1 or 3, free head RLC | 10S | |
| TT1 | Segments 1, 2, 3 | 10S | |
| TT2 | Segments 1, 3 | 10S | |



165 The table and cartoon summarize the head-head, head-tail and tail-tail interactions in 10S myosin, based on the 3D
166 reconstruction. The cartoon corresponds to the reconstruction in Fig. 5A and B. Blocked and free heads are represented
167 by red and green, respectively. Yellow dots represent mesa of blocked head. MD, motor domain; ELC, essential light
168 chain; RLC, regulatory light chain; SH3, SRC homology 3 domain; Con, converter. TT1 and TT2 mark initial points of
169 contact between segments 1 and 3, and segments 1, 2 and 3, respectively. From these initial points, these segments run
170 closely together and may interact along much of their lengths. Note: corresponding domains in the two heads have
171 different apparent shapes and sizes in this 2D representation of the 3D reconstruction, in which the domains are viewed
172 at different angles (cf. Fig. 5A).

173

8

174    tail. The interaction between the blocked (B) and free (F) heads (BF) has been described before [1,
175    32], and is confirmed here. Eight putative interactions between the heads and the tail (T) have not
176    previously been observed in 3D: these include the free head with tail segments 1 and 3 (TF), and
177    the blocked head with segments 1, 2 and 3 (TB). Interactions between different segments of the
178    tail were also observed (TT).

179    ***Head-head interactions:*** As described previously, the overall conformation of the IHM is
180    produced by the blocked and free heads (red and green respectively in Fig. 3) interacting with
181    each other (BF, blue arrow in Fig. 5A). The atomic model from this earlier work (PDB1i84) can be
182    fitted well into the volume (Fig. 4, Movie 2).

183    ***Tail-head interactions:*** Three interactions are found between segment 2 of the tail and the
184    blocked head as the tail wraps around its perimeter (Fig. 5A). TB2 is the interaction between tail
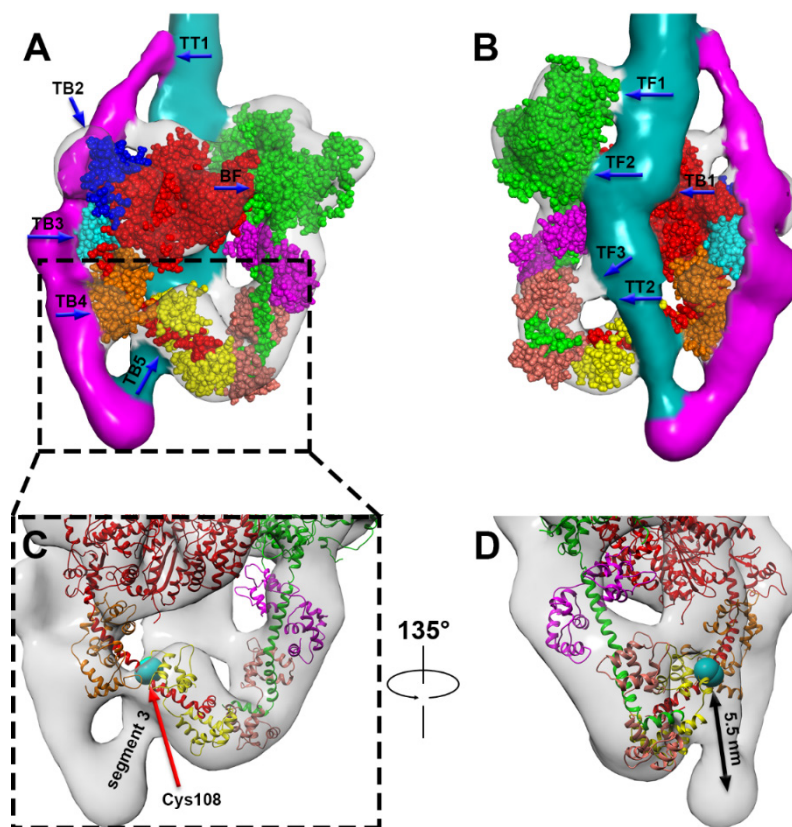


**Figure 5. Interactions between the tail and heads in 10S myosin.** (A) Front view shows the interactions between segments 2 (magenta) and 3 (cyan) and the blocked head (TB2, TB3, TB4, TB5), between the two heads (BF), and between segment 2 and the other tail segments (the interaction extends upwards from TT1). TB2 is between the SH3 domain (blue) in the blocked head and segment 2, which lies under it. TB3 is between segment 2 and the converter domain (cyan) of the blocked head. TB4 is between segment 2 and the ELC (orange) of the blocked head. TB5 is between segment 3 and the blocked head RLC. (B) Back view shows the interaction between the free head and the tail (TF1, TF2, TF3), between segments 1 and 3 (unresolved from each other) and the blocked head (TB1), and between segments 1 and 3 (starting at TT2). Interaction TF1 is between the actin-binding loop in the free head and the tail, while TF2 is between the free head and segment 1 or 3. TF3 may represent merging of tail and blocked head densities and not be a real interaction (see text). TB1 is an extended interaction between the blocked head and segment 1 and/or segment 3. (C) Magnified view of TB5. Cys108 is represented by a cyan sphere. (D) The view in (C) is rotated 135º to visualize the geometric relationship between Cys108 and segment 3.

185    segment 2 and the blocked head SH3 domain (blue in Fig. 5A). The blocked head is likely to be
186    stabilized by this interaction. Interaction TB3 was found between segment 2 and the converter
187    domain of the blocked head (cyan in Fig. 5A). The third interaction, TB4, was found between
188    segment 2 and the ELC of the blocked head (orange in Fig. 5A).

189    Four interactions were observed between the tail and the underside of the heads (Figs. 5A, B,
190    Table 1). TB1 is an extensive interaction, where the tail (including segments 1 and 3, which are not
191    resolved from each other) runs over the back-surface of the blocked head motor domain (Fig. 5B).
192    TB5 involves interaction between the RLC of the blocked head and segment 3, close to the second
193    tail hinge point (Fig. 5A). TF1 occurs between the tail and the actin-binding loop of the free head,
194    while TF2 is the interaction between tail segment 1 or 3 and the upper 50K domain of the free
195    head. TF3 is a possible interaction between the tail and the free head RLC, but could alternatively
196    represent low resolution merging of densities without actual contact (Fig. S4; see Discussion).
197    These interactions between the tail and the free head were not reported in 2D analysis of smooth
198    muscle myosin [9, 35], probably because the tail in these interactions is superimposed on the
199    heads and cannot be identified in the 2D images.

200    ***Tail-Tail Interactions:*** In addition to the head-tail interactions, two regions of contact were found
201    between the different segments of the tail. TT1 is an extensive interaction starting at the top of the
202    IHM (Fig. 5A), where segment 2 merges with segments 1 and 3, and continuing up as a triple
203    coiled-coil complex [9]. A second extensive interaction appears likely between segments 1 and 3
204    (unresolved from each other), as they pass together over the blocked head (Fig. 5B). This
205    interaction starts at TT2, where the first part of segment 3 (cyan in Fig. 5B), would merge with the
206    initial portion of S2 (not visible in the reconstruction, as discussed earlier). Other parts of the tail
207    (the region of segment 2 peeling away from the triple segment and wrapping around the blocked
208    head, and the start of segment 3 after the second tail hinge) exist as single coiled-coils, consistent
209    with their narrower diameter in the reconstruction.

## Heterogeneity in the reconstruction

211    The flexibility of the merged tail segments extending beyond the head region is visualized in raw
212    images, and was investigated using 2D classification by Burgess *et al.* [9], who showed that the tail
213    flexed within a range of ~ 60° where it left the heads. The heads are also flexible, though more rigid
214    than the tail. 3D classification was performed to explore flexibility and heterogeneity in the 10S
215    molecules. 15833 particles were classified into 6 classes using RELION [40] (Figs. 6, S5). Classes
216    3 and 4, comprising 51% of the particles, exhibited very similar structures (Fig. 6C, D). Both tail
217    and IHM were visualized clearly in 3D reconstructions and could be fitted well with the 3D atomic
218    model of chicken smooth muscle myosin. The particles in these classes were combined and used
219    for 3D refinement to produce the reconstruction described above. The other 4 classes were
220    smaller and exhibited different tail and IHM structures in their reconstructions (Fig. 6A, B, E).

221    The classification results suggest that the tail plays a crucial role in stabilizing the compact
222    structure of 10S myosin. When the tail can be traced explicitly (classes 3, 4 and 6), the IHM shows
223    more consistent structural features than in the other three classes. 30% of myosin molecules
224    (classes 1, 2 and 5) had flexible or disordered tails. Segment 2 density was discontinuous in class
225    1 and almost completely disappeared in classes 2 and 5, and the second hinge point was not
226    visible in the latter two (Fig. 6B, E). Although these classes exhibited a similar basic asymmetric
227    organization of heads, their IHM structure was somewhat varied, and the atomic model of the IHM
228    (PDB 1I84) could not be docked into them very well. This implies that the tail directly influences the

229 stability of the molecules, helping to maintain a compact structure: the weak interaction between
230 the blocked and free heads is strengthened by the interactions of the heads with the tail. Disruption
231 of these interactions results in conformational changes and less compact myosin molecules. Class
232 6 molecules exhibited less detail than classes 3 and 4, and were therefore also excluded from the
233 final reconstruction.

234
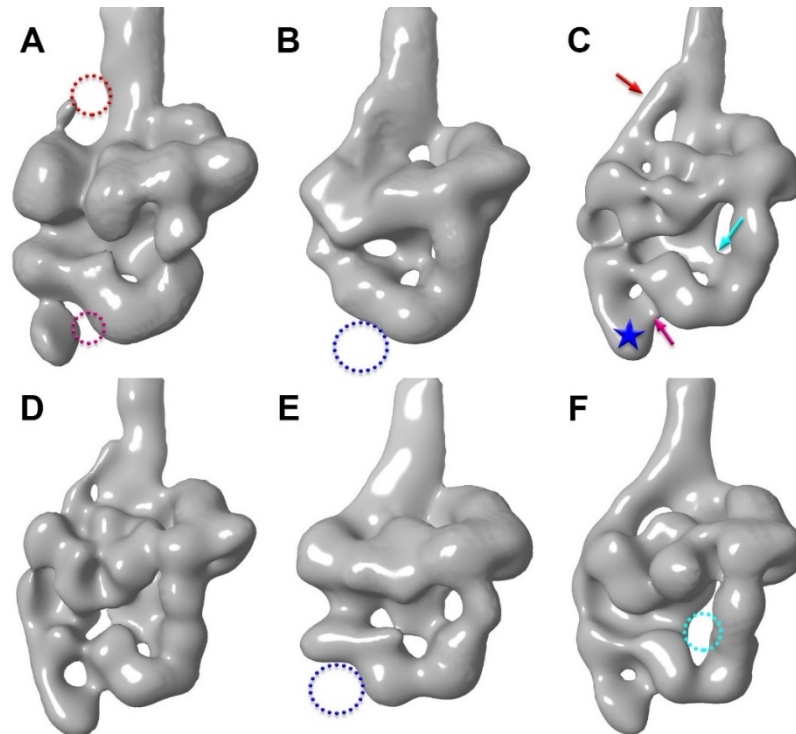


**Figure 6. Heterogeneity in the reconstruction.** 3D classification using RELION produced six classes of conformation (A-F show classes 1-6 respectively), showing that the 10S myosin molecules are quite heterogeneous. (A) The tail density partially disappeared in some regions (red dotted circles, *cf.* red arrows in (C), where it is visible). (B) The tail cannot be explicitly identified in this reconstruction and the second hinge point (star in (C)) is missing (blue circle). The reconstructions in (C) and (D) showed similar structural features, with both the interacting heads and the tail clearly visible. (E) Segment 2 around the blocked head is not visible, and the second hinge point is absent (blue circle), as in (B). (F) The tail wraps around the blocked head, but the density present in (C) (cyan arrow) and (D) is absent (cyan circle).

## Discussion

236 While the head interactions that define the IHM in 10S myosin have previously been studied in
237 detail [1, 32], the role of the tail in inhibiting function has not been well appreciated. Our
238 reconstruction shows the 3D organization of the tail for the first time, providing crucial insights into
239 the mechanism of inhibition that underlies the storage function of the folded molecule. The
240 densities of the tail running across and wrapping around the two heads can be traced explicitly
241 (Fig. 3D, E, F, Movie 2), in contrast to earlier studies where the tail could not be identified [1] or
242 was not analyzed in 3D [9]. These earlier studies illustrate the difficulties of visualizing the myosin
243 tail by cryo-EM and the ease with which it can be seen by negative staining, our technique of
244 choice (see [33, 34] and Methods). While the resolution of the reconstruction is not high (due partly

245 to flexibility of the molecule), we could easily detect the different domains of the myosin heavy
246 chain and light chains, revealing steric blocking of specific regions of the heads by the tail that
247 explains how the molecule is so effectively switched off in the quiescent state [31]. Fitting the
248 atomic model of the IHM (PDB 1i84) to the reconstruction further refined our interpretation of
249 interactions [37][]. The most important finding from our study is that interactions of the tail with the
250 heads and with itself, combined with interactions between the heads, block all four key functional
251 characteristics of 10S myosin: 1. ATPase activity, by head-head and head-tail interaction; 2. Actin
252 binding, by head-head and head-tail interaction; 3. Activation by phosphorylation, through RLC-tail
253 interaction; and 4. Filament formation, by tail-tail interaction. Inhibition of every aspect of myosin
254 function appears to be nature's failsafe method for conserving energy in the inactive state.

255 **The tail plays a central role in switching off 10S myosin activity**

256 The reconstruction shows evidence for eight possible interactions between the tail and the heads
257 in 10S myosin (Table 1). Five of these involve the blocked and three the free head, suggesting that
258 the blocked head is the more stable [9]. All eight interactions may be important in creating a fully
259 inhibited 10S molecule, but two stand out as being the most stable.

260 *1. Segment 1-blocked head interaction:* Interaction between the blocked head and segment 1
261 (subfragment 2; TB1; Fig. 5B) appears to be one of the most fundamental interactions of the
262 inhibited state, helping to maintain the blocked head in its folded-back conformation. This is
263 suggested by its occurrence not only in myosin filaments and 10S myosin, but also in HMM [9]. In
264 HMM, the free head preferentially detaches from the IHM in some molecules, while the blocked
265 head remains bound to subfragment 2 [9]. The free head also detaches more readily than the
266 blocked head in full-length (10S) myosin [9] (Fig. S6) and filaments [41], further suggesting
267 stabilization of the blocked head by its binding to subfragment 2. Smooth muscle HMM constructs
268 with different tail lengths are switched off only when the tail is equal to or greater in length than the
269 head [42]. This is approximately the distance segment 1 must travel from its origin at the head-
270 head junction to its interaction (TB1) with the blocked head mesa (Fig. 5B). This supports the view
271 that the S2-blocked head interaction plays a critical role in inhibition [23].

272 *2. Segment 3-blocked head RLC interaction:* We suggest that interaction TB5 (Fig. 5A),
273 between segment 3 and the blocked-head RLC, is the strongest (and therefore the key) interaction
274 that pins the tail to the heads, creating the folded, inhibited structure of 10S myosin, and helping to
275 hold segments 2 and 3 in position where they interact with key sites on the blocked and free
276 heads. The existence of this interaction is supported by photo cross-linking, showing that Cys108,
277 in the C-terminal half of the RLC, is cross-linked to the tail between Leu1554 and Glu1583, which
278 lie in segment 3 [35]. The tail must therefore fold back on to the light chain domain. The calculated
279 distance from Glu1535 to Lys1568 (the middle residue in the cross-linking region) is ~ 48 Å,
280 assuming 1.485 Å rise per residue along a coiled-coil. In the reconstruction, the distance measured
281 from Glu1535 (hinge 2 [9], star in Fig. 3D) to Cys108 (cyan in Fig. 5C, D; Movie 3) in the blocked
282 head RLC is similar (~ 55 Å). In the crosslinking studies, only one of the two RLCs is crosslinked to
283 the tail [35, 43]. This is readily explained by the reconstruction, which shows that only blocked
284 head Cys108 is close enough to the tail for crosslinking (Movie 3).

285 The crucial importance of TB5 to the folded structure is illustrated by previous biochemical and EM
286 observations of 10S myosin. **(1)** When observed by rotary shadowing or negative staining,
287 molecules that are not crosslinked by glutaraldehyde show a loosely folded structure, in which the
288 only (and therefore strongest) intramolecular contact occurs between the start of segment 3 and

12

289    the neck region (containing the RLC) of one head [10, 35]: the other interactions observed in our
290    work are presumably weaker, and, in the absence of the glutaraldehyde treatment that we used,
291    are disrupted by binding of the molecule to the negatively charged mica surface used for
292    shadowing [26]. **(2)** In *Dictyostelium* and many insect flight muscle myosin II molecules, segment 3
293    does not bind to the blocked head; in these molecules, the tail and free head are quite flexible (Fig.
294    S6A, C). **(3)** Segments 1 and 2 of smooth muscle myosin are together 1020 Å long [9]. Myosin II's
295    from amoeba (*Acanthamoeba castellanii*) and yeast (*Schizosaccharomyces pombe*) are much
296    shorter than smooth muscle myosin, with total tail lengths of 870 and 910 Å, respectively [26].
297    They thus lack segment 3 entirely and the last 100-150 Å of segment 2. Neither of these myosins
298    folds [26], further supporting the idea that segment 3 is essential for forming the 10S structure. **(4)**
299    Biochemical observations also demonstrate the importance of the RLC for folding. The folded
300    conformation fails to form when the RLC is removed [44] or replaced by skeletal RLC [45].
301    Experiments with chimeric smooth/skeletal RLCs show that native smooth N- and C-terminal lobes
302    are both required for formation of 10S myosin [45]—the C-terminal lobe for full binding of the RLC
303    to the heavy chain, and the N-terminal for folding. TB5 in our reconstruction shows segment 3
304    positioned over the C-terminal lobe and immediately next to the N-terminal lobe of the blocked
305    head RLC, providing a structural explanation for these findings (Fig. 7E, F). The first twenty-four
306    residues of the RLC are absent from the N-terminus in PDB 1i84, probably due to mobility. This
307    region (dubbed the phosphorylation domain (PD) [46]) stabilizes tail folding in smooth muscle
308    myosin [47]. We have estimated the location of these residues by superimposing the RLC of
309    scallop (PDB 3JTD, which includes eleven additional N-terminal residues) on to the smooth muscle
310    structure (Fig. S7). Residues 1-11 in scallop (14-24 in smooth muscle) of the blocked head RLC
311    appear to contact segment 3, consistent with this stabilizing interaction. Based on sequence
312    analysis and modeling, it has been suggested that the N-terminal 24 amino acids, including a
313    specific group of positively charged residues, may lie over a cluster of negatively charged residues
314    in segment 3, trapping this region of the tail on top of the RLC C-lobe and accounting for the
315    strength of this interaction [35]. An alternative proposal is that these N-terminal RLC residues
316    interact with helix A of the ELC in the switched off molecule [48].

317    ***3. Other interactions:*** While the blocked head RLC interacts with segment 3, a putative
318    interaction (TF3) with the free head RLC is less certain (Fig. 5C, D). The density in this region is
319    very weak and fitting of PDB 1i84 suggests that there is no RLC density to fill the volume (Fig. S4);
320    the relatively uniform cylindrical tail also lacks such density (Figs. 4, 5, S3, S4). This apparent
321    interaction could therefore represent low resolution merging of the tail and head densities without
322    actual contact. TF3 is close to the point where the first portion of segment 1, missing from the
323    reconstruction, as discussed earlier (Figs. 3E, S4), would meet segment 3. This may account for
324    the sudden widening of the tail at this location (Fig. 5B), leading to possible fusion with the RLC
325    density.

326    In addition to interacting with the heads, the folded tail appears to interact with itself, where
327    segments 1 and 3 run next to each other over the blocked head (interaction starting at TT2; Fig.
328    5B), and at the top of the reconstruction, where all three segments form a compact, rod-shaped
329    structure, extending upwards from TT1 (Figs. 3, 5A). These interactions appear to play an
330    essential role in the function of 10S myosin. First, folding sequesters the tail, inhibiting
331    polymerization with other tails to form filaments, the active form of myosin II in cells. Second,
332    extending up from the TT1 contact site, the complex of the three tail segments is quite flexible and
333    can be significantly curved [9]. However, the interacting-heads structure remains relatively rigid.
334    The TT1 contact site may function as a lock, preventing conformational changes in the curved rod

335    complex from being transferred to the heads, thus helping to maintain their inhibited state. This is
336    suggested by our observation that in the absence of TT1, as in *Dictyostelium* (Fig. S6B) and many
337    insect indirect flight (Fig. S6D) muscle myosin molecules [26], the free head frequently detaches
338    from the blocked head. The interaction between segments 1 and 3 starts at TT2. Proximity of TT2
339    to interaction TB5 (Fig. 5) may stabilize the interaction between segment 3 and the RLC in the
340    blocked head.

341    **Tail segments 2 and 3 stabilize the IHM in 10S myosin**

342    The atomic model of the IHM (PDB 1i84, based on 2D crystals of HMM [1]) fits well into the head
343    densities of the reconstruction, without the need for any substantial change in head structure (Fig.
344    4D-F, Movie 2). This shows that binding of tail segments 2 and 3 (absent from HMM) to the heads
345    in 10S myosin is not required to generate the head-head interactions, and that it does not
346    significantly distort them. However, the frequency of formation of the interacting-heads structure in
347    HMM, containing only the first third of the tail and having only one interaction between the tail and
348    heads (TB1 in Fig. 5B), and the stability of the free head in HMM, are both lower than in full-length
349    (10S) myosin [9]. Thus, these segments stabilize the head-head interactions, the compact
350    structure and the inhibited function of 10S myosin. Several observations support this view: **(1)** a
351    subset of the reconstructions that lack some of the tail density features correspondingly had a
352    more varied head structure (Fig. 6A, B, E). **(2)** Myosin from *Dictyostelium* [26], which lacks
353    segment 2 wrapping around the blocked head [26], showed more frequent cases of non-interacting
354    heads (Fig. S6C, D). **(3)** Myosin molecules from insect flight muscle frequently behaved similarly
355    (Fig. S6A, B). These observations suggest that the interactions of all three tail segments with the
356    heads are crucial in fully stabilizing the structure of 10S myosin.

357    **Intramolecular interactions in thick filaments and single molecules: similarities and**
358    **differences**

359    10S myosin and thick filaments share several interactions. These include BF, TB1, TB2, TB3 and
360    TF1 (Fig. 5, Table 1). Conservation of these interactions between filament and molecule suggests
361    that they play an important role in the inhibited state of myosin. In both filament and molecule, it is
362    thought that the BF interaction, between the two heads, constrains movement of the converter
363    domain of the free head, inhibiting phosphate release, and blocks actin-binding by the blocked
364    head [1, 23]. TB1 occurs between segment 1 and/or segment 3 and the blocked head where these
365    two segments run over its motor domain (Fig. 5B). In filaments, where the tail is not folded [23],
366    and in HMM, where segments 2 and 3 are absent [9, 35], this blocked head-S2 interaction is also
367    present, supporting the view that TB1 involves S2, and consistent with data showing that
368    subfragment 2 binds to subfragment 1 in solution [49]. The reconstruction suggests that in 10S
369    myosin, segment 3 also binds to the blocked head motor domain. The tail is wider where it runs
370    over the blocked head than at the start of segment 3, where it is a single α-helix (Fig. 5B),
371    suggesting that segment 3 runs next to segment 1 over the blocked head. This double interaction
372    with the blocked head would presumably help to stabilize the IHM of the folded molecule. TB2 (Fig.
373    5A) occurs between segment 2 and the SH3 domain (blue in Fig. 5A) of the blocked head. A
374    related interaction is observed in relaxed thick filaments, between the SH3 domain of the blocked
375    head and the tail from the next pair of heads away from the bare zone [23, 50]; however, in this
376    case the interaction involves segment 1, and its polarity is the reverse of that in the 10S molecule.
377    TB3 occurs between segment 2 and the converter domain of the blocked head (Fig. 5A). As with
378    TB2, a similar interaction (but with reverse polarity) occurs between the converter domain and
379    segment 1 of the neighboring tail in thick filaments [23]. The fifth interaction, TF1, occurs between

14

380  the tail and the free head actin-binding loop in 10S myosin. A similar interaction between S2 and
381  the actin-binding loop has been suggested in tarantula thick filaments [51], suggesting that TF1
382  also involves S2.

383  The other interactions in 10S myosin are unique to the folded structure. These tail-head and tail-tail
384  interactions are presumably important specifically to the switched-off, folded structure, which
385  underlies its storage and transport function. The compact structure would make transport more
386  efficient through the crowded intracellular environment, while inhibition of ATPase and actin
387  binding would minimize energy use and futile binding to actin filaments during transport.

### 10S myosin is switched off by steric blocking of ATPase and actin-binding sites on both heads

388
389

390  EM studies of 10S smooth muscle myosin [1, 32] suggested that inhibition was achieved by
391  different mechanisms in the two heads: (1) by preventing actin binding in the blocked head; and (2)
392  by inhibiting ATPase activity in the free head [1]. But they provided no information on the possible
393  role of the tail in inhibition. Our results suggest that the tail plays a central role in switching off
394  activity, such that *both* of these inhibitory mechanisms occur in *both* heads—but in different ways.

395  *1. Inhibition of actin binding:* Part of the actin-binding interface of the blocked head is obstructed
396  by interaction with the free head, as shown previously [1] (interaction BF; red ellipse in Fig. 7C). In
397  the free head, it is clear that actin-binding is also sterically blocked, through interaction of its actin-
398  binding loop with the tail (interaction TF1; Fig. 5B; green ellipse in Fig. 7C, D), and by interference
399  of the bundle of three tail segments (projecting up from TT1) with the free head actin-binding
400  interface. Thus, each head would be prevented from binding to actin by distinct steric blocking
401  mechanisms, one involving the tail and one the other head.

402  *2. Inhibition of ATPase activity:* Similarly, ATPase activity of 10S myosin appears to be inhibited
403  not only in the free, but also the blocked head, by stabilization of the converter domain of each,
404  preventing phosphate release (cf. [52]). In the free head, the converter is immobilized by binding to
405  the blocked head [1] (interaction BF; Fig. 5A; blue ellipse in Fig. 7A). In the blocked head, the
406  converter may also be immobilized—in this case by binding to segment 2 of the tail as it wraps
407  around the head (interaction TB3, Fig. 5A; red ellipse, Fig. 7A, B).

408  Inhibition of ATPase activity in both heads of 10S myosin would help explain a previously puzzling
409  observation. Release of ATP hydrolysis products is ten times slower in 10S myosin than in HMM
410  (0.0002 $S^{-1}$ and 0.003 $S^{-1}$ respectively) [31]. If the free head is inhibited in both (by binding to the
411  blocked head), blocked head product release must be more inhibited in 10S myosin than in HMM.
412  This could be explained by interaction of tail segment 2 with the blocked head converter in 10S
413  myosin but not HMM, where it is missing. As mentioned previously, tail wrapping around the heads
414  may also stabilize the basic head-head interaction of the IHM [1], enhancing the inhibitory effect of
415  the two heads on each other in the 10S molecule.

416  We conclude that phosphate release and actin-binding are both inhibited in both heads, which can
417  explain why 10S myosin is completely switched off [31], making it so well suited to its energy-
418  conserving storage function in cells. The folded tail plays a critical role in this inhibition.

419  In thick filaments [23], both actin binding and ATPase are also sterically inhibited in both heads,
420  again in different ways. Blocked-head actin binding is inhibited by interacting with the free head, as
421  with 10S myosin, while the free-head is inhibited by orientation of its actin-binding face towards the
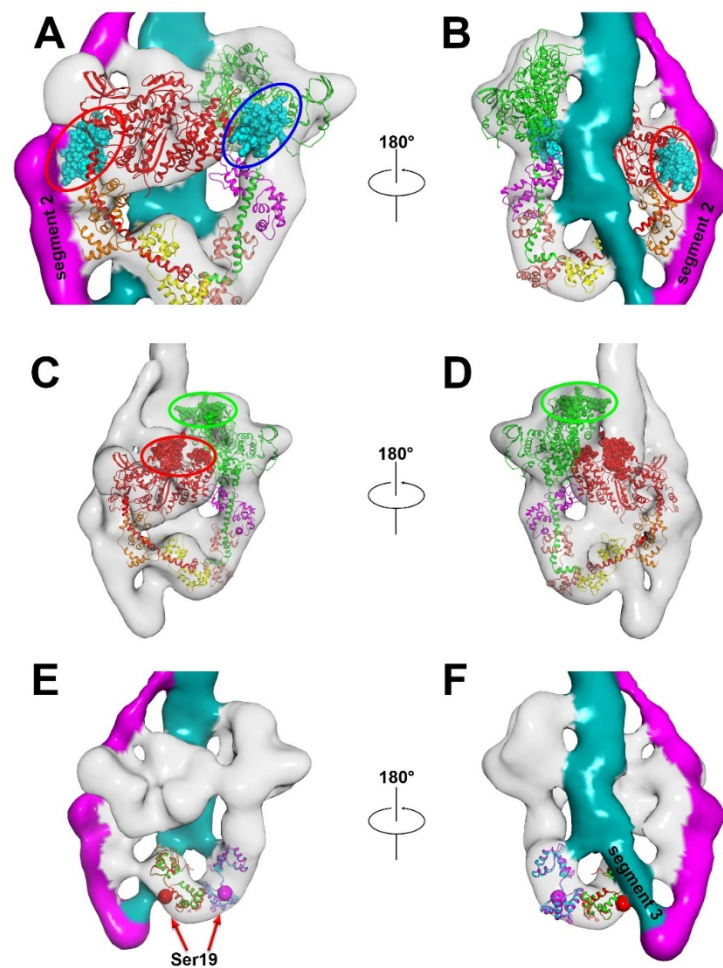
**Figure 7. Inhibition mechanism of phosphate release and actin binding in the two heads.** (A) Phosphate release in the blocked head is inhibited by interaction between its converter domain (cyan within red ellipse) and segment 2, and in the free head by interaction between its converter domain (cyan within blue ellipse) and the blocked head. (B) Back view, rotated 180º from (A). (C) and (D) Front and back views show actin-binding loop (red ellipse) in the blocked head sterically blocked by the free head, and actin-binding loop (green ellipse) in the free head blocked by interacting with the tail. (E) and (F) Front and back views showing steric blocking of Ser19 (red sphere) by segment 3 in the blocked head RLC, but not in the free head RLC (magenta sphere; see Movie 4).

422    thick filament backbone, away from actin. Both converters are also inhibited [23], impeding
423    ATPase activity: in the free head by binding to the blocked head, as in 10S myosin; in the blocked
424    head by interacting with S2 from the neighboring crown, as discussed above [23]. The greater
425    number of interactions found in 10S myosin than in thick filaments suggests that the IHM of 10S
426    myosin is more stable than in thick filaments, consistent with the greater inhibition observed in
427    molecules [21, 31].

428    **The central role of the tail in activation of 10S myosin**

429    Smooth and nonmuscle 10S myosins are activated *in vitro* by phosphorylation of their RLCs.
430    Under physiological ionic conditions this causes conversion to the 6S (unfolded) conformation [10,
431    15], which can form filaments, hydrolyze ATP and bind to actin. Our reconstruction provides insight
432    into the mechanisms of these processes. Biophysical data suggest that phosphorylation of 10S

16

433    myosin is a sequential process in which one RLC is phosphorylated more readily than the other,
434    and it has been proposed that this might result from an asymmetric arrangement of the myosin
435    heads [53, 54] (others have suggested that phosphorylation is random, but the starting myosin in
436    those studies may not have been in the 10S conformation [55, 56]). The reconstruction reveals not
437    only asymmetry of the heads (as previously described), but also dramatically different
438    environments of their phosphorylation sites, which would readily account for a sequential
439    phosphorylation process. Ser19 in the free head RLC is completely accessible to MLCK and would
440    be easily phosphorylated. In the blocked head, Ser19 is sterically hindered by segment 3 of the tail
441    (interaction TB5; Figs. 7E, F, Movie 4), which would hamper access of MLCK. Thus, the free head
442    RLCs would be phosphorylated first, and blocked head RLCs later [53, 54, 57, 58]. A similar
443    difference in accessibility of MLCK to the phosphorylatable serines is observed in tarantula
444    filaments due to differing steric environments in the filament [41].

445    Biophysical measurements show that both RLCs must be phosphorylated for complete transition of
446    the 10S to the 6S conformation [57, 58], and for significant activation of ATPase activity [53]. This
447    suggests that phosphorylation of the blocked head RLC (occurring second) must ultimately
448    determine unfolding, and that singly phosphorylated molecules would remain mostly folded and
449    relatively inactive. The immediate proximity of Ser19 on the blocked head RLC to interaction
450    TB5—which we suggested earlier is the critical interaction for creating the folded state (Fig. 7E,
451    F)—would explain how phosphorylation of this serine could be the key step that causes tail
452    unfolding. This proximity suggests a direct (rather than allosteric) effect of phosphorylation on the
453    binding of segment 3: decreased positive charge on the RLC would weaken its interaction with the
454    negatively charged region of segment 3, favoring unfolding of the tail [35]. Extension of RLC helix
455    A upon phosphorylation [46], or changes in ELC-RLC interaction affecting the conformation of the
456    light chain domain [48, 59], might also contribute to the loss of interaction with segment 3.
457    Importantly, heavy meromyosin, which lacks segments 2 and 3, requires phosphorylation of only
458    one of its two heads for activation [60]: in this case TB5 does not exist, and phosphorylation of a
459    single head is sufficient to break the weaker head-head interaction in HMM. The requirement for
460    phosphorylation of both heads in 10S myosin (one of which is sterically inhibited) for full activation
461    may be another mechanism by which the cell conserves energy in the quiescent state. If any
462    MLCK molecules in the cell are $Ca^{2+}$-insensitive (e.g. through proteolysis or other damage),
463    resulting RLC phosphorylation will occur preferentially on the free head, but this will not activate
464    the molecule. Only when intracellular $Ca^{2+}$ levels rise will there be sufficient activated MLCK to
465    phosphorylate the blocked head RLC as well, with concomitant unfolding of the 10S structure.

466    Based on the above observations and previous work, we propose the following mechanism for
467    regulating 10S myosin activity in cells. **1.** At low intracellular $Ca^{2+}$, both heads are
468    dephosphorylated, and the molecule is in the 10S conformation, in which ATPase activity and actin
469    binding are inhibited by the mechanisms discussed earlier. **2.** With increased $Ca^{2+}$, MLCK is
470    activated, and first phosphorylates the unobstructed RLC of the free head. This may alter the
471    conformation of the light chain domain of this head, weakening interaction of the free head with the
472    blocked head and the tail, while retaining the overall folded conformation and relatively low
473    ATPase activity of the molecule [9, 48, 53, 57-59]. **3.** The less accessible blocked head RLC is
474    then phosphorylated. This could result from the weakening of the IHM just mentioned, or from
475    "breathing" of the intact 10S structure, which transiently exposes blocked head Ser19 (we assume
476    that the interactions we have described are relatively weak and in equilibrium between interacting
477    and non-interacting states). There is also evidence that the RLCs may interact with each other and
478    with the flexible initial portion of subfragment 2, stabilizing the conformation of this region of the

479 IHM [23, 28, 50]. Phosphorylation of the free head RLC may disrupt these interactions, leading to
480 increased local flexibility and greater accessibility of Ser19 on the blocked head RLC. **4.**
481 Phosphorylation of the blocked head phosphorylation domain weakens or abolishes its interaction
482 (TB5) with the negative charge cluster on segment 3 due to decreased charge attraction. **5.** With
483 breakage of TB5 (the key interaction required for the folded state), the binding of segments 1 and 2
484 to the heads is destabilized, allowing the tail to become fully extended. **6.** Loss of head-tail
485 interactions during tail unfolding may further destabilize previously weakened head-head contacts,
486 promoting separation of the heads. **7.** The extended tails now interact to form filaments, actin-
487 binding sites on both heads are exposed, and inhibitory interactions of the converter domains are
488 lifted, leading to full actin-activated ATPase activity and filament sliding.

## Materials and Methods

## Electron microscopy

491 Smooth muscle myosin II from turkey gizzard was purified according to [61]. Smooth muscle
492 myosin has similar structural and functional properties to nonmuscle myosin II and is a convenient
493 source for our experiments on the 10S structure [10]. Myosin molecules in 0.15 M NaAc, 1 mM
494 EGTA, 2.5 mM $MgCl_2$, 0.5 mM ATP, 10 mM MOPS, pH 7.5 were negatively stained at 10 nM
495 concentration using 1% (w/v) uranyl acetate [33]. Negative staining is a simple and powerful
496 technique for obtaining 3D structural data at moderate resolution. While it does not provide the
497 high resolution possible with cryo-EM, it is more than adequate for revealing structure and
498 interactions at the domain level and was therefore our method of choice (see [33, 34]); the detail
499 observed in our reconstruction was sufficient to provide multiple new insights into the mechanism
500 of inhibition in the 10S molecule. Carbon films were pretreated with UV light to optimize stain
501 spreading [2, 62]. Molecules were lightly crosslinked in solution at room temperature for 1 min with
502 0.1% glutaraldehyde before staining [2, 35]. This was designed to minimize distortion caused by
503 binding to the carbon surface and drying of the stain, and does not significantly alter the structure
504 of the molecules at the resolution of our studies [2, 35]. 200 micrographs were recorded under low
505 dose conditions on a Philips CM120 electron microscope at 120 kV with a 2K x 2K CCD camera
506 (F224HD, TVIPS GmbH) at a pixel size of 3.7 Å (nominal 45,000 magnification). These
507 micrographs were used for 3D reconstruction and refinement. 100 pairs of micrographs of tilted
508 (50º) and untilted (0º) grids were collected at 5.4 Å/pixel (nominal magnification 37,000) for random
509 conical tilt reconstruction.

## Image processing

511 Initial model from random conical tilt. No complete 3D model is available for 10S myosin II to use
512 as a reference for 3D reconstruction. To exclude model bias, we implemented the random conical
513 tilt method [36] to create a starting model, using SPIDER [63]. 13,675 pairs of particles were
514 interactively selected from the 100 tilted and untilted micrographs using the program JWEB in
515 SPIDER. 2D classification was performed for the untilted particles. Four classes of particle with
516 similar views in the class averages were chosen for further analysis. For each class, the Euler
517 angle of each particle from the tilt images was calculated based on the tilt angle and the azimuthal
518 angle from 2D classification. Back projection was carried out to compute the 3D reconstruction.
519 Finally, the four class averages were rotated to make the tail parallel to the y-axis. The obtained
520 azimuthal angles were used to modify the Euler angles and to merge particles from the chosen
521 four classes, and the model was built using the merged data set.

522 2D classification and 3D reconstruction. The folded tail of 10S myosin protruding beyond the heads
523 is flexible, and also rotates (within a 60º range) about its junction with the heads [9]. To simplify
524 analysis, only particles with an unbent tail pointing straight up from the head-head junction were
525 chosen for image processing. Particles with dimensions 150 x 150 pixels, including both heads and
526 a small portion of the protruding tail, were manually selected using EMAN [64], and then low-pass
527 filtered to 20 Å. All subsequent image processing was carried out with RELION [40]. Four rounds
528 of 2D classification were performed. Bad or low-resolution particles with smeared densities were
529 removed after each round. The remaining 15833 particles were subjected to 3D classification into
530 6 classes. Classes 1, 2 and 5 showed variable appearances of the tail and heads. Classes 3 and 4
531 had similar 3D reconstructions and were combined for refinement. The resolution of the refined 3D
532 reconstruction was estimated to be 25 Å (Fig. S2). Class 6 molecules showed less detail than
533 classes 3 and 4, and were excluded from the final reconstruction

534 Atomic fitting. The atomic model of the interacting heads of chicken smooth muscle myosin (PDB
535 1I84) [1] was docked into the 3D reconstruction using rigid-body fitting in CHIMERA [65] (Fig. 4).
536 Molecular dynamics flexible fitting was not attempted owing to the low resolution. Densities outside
537 of the heads were attributed to the three segments of the tail. According to 3D classification (Fig.
538 6), S2 in the 3D reconstruction was quite flexible. We therefore chose not to fit an atomic model of
539 S2 to the reconstruction.

## Acknowledgments

## Competing interests

549 The authors declare no competing interests.

550

551

552

553

554

555

## References

1. Wendt, T., Taylor, D., Trybus, K.M., and Taylor, K. (2001). Three-dimensional image reconstruction of dephosphorylated smooth muscle heavy meromyosin reveals asymmetry in the interaction between myosin heads and placement of subfragment 2. Proceedings of the National Academy of Sciences of the United States of America *98*, 4361-4366.

2. Jung, H.S., Komatsu, S., Ikebe, M., and Craig, R. (2008). Head-head and head-tail interaction: a general mechanism for switching off myosin II activity in cells. Mol Biol Cell *19*, 3234-3242.

3. Yang, S., Woodhead, J.L., Zhao, F.Q., Sulbaran, G., and Craig, R. (2016). An approach to improve the resolution of helical filaments with a large axial rise and flexible subunits. J Struct Biol *193*, 45-54.

4. Geeves, M.A., and Holmes, K.C. (1999). Structural mechanism of muscle contraction. Annual review of biochemistry *68*, 687-728.

5. Vicente-Manzanares, M., Ma, X., Adelstein, R.S., and Horwitz, A.R. (2009). Non-muscle myosin II takes centre stage in cell adhesion and migration. Nat Rev Mol Cell Biol *10*, 778-790.

6. Tajsharghi, H., and Oldfors, A. (2013). Myosinopathies: pathology and mechanisms. Acta Neuropathol *125*, 3-18.

7. Moore, J.R., Leinwand, L., and Warshaw, D.M. (2012). Understanding cardiomyopathy phenotypes based on the functional impact of mutations in the myosin motor. Circulation research *111*, 375-385.

8. Suzuki, H., Onishi, H., Takahashi, K., and Watanabe, S. (1978). Structure and function of chicken gizzard myosin. Journal of biochemistry *84*, 1529-1542.

9. Burgess, S.A., Yu, S., Walker, M.L., Hawkins, R.J., Chalovich, J.M., and Knight, P.J. (2007). Structures of smooth muscle myosin and heavy meromyosin in the folded, shutdown state. Journal of molecular biology *372*, 1165-1178.

10. Craig, R., Smith, R., and Kendrick-Jones, J. (1983). Light-chain phosphorylation controls the conformation of vertebrate non-muscle and smooth muscle myosin molecules. Nature *302*, 436-439.

11. Suzuki, H., Kamata, T., Onishi, H., and Watanabe, S. (1982). Adenosine triphosphate-induced reversible change in the conformation of chicken gizzard myosin and heavy meromyosin. J Biochem *91*, 1699-1705.

12. Trybus, K.M., Huiatt, T.W., and Lowey, S. (1982). A bent monomeric conformation of myosin from smooth muscle. Proc Natl Acad Sci U S A *79*, 6151-6155.

13. Cross, R.A., Cross, K.E., and Sobieszek, A. (1986). ATP-linked monomer-polymer equilibrium of smooth muscle myosin: the free folded monomer traps ADP.Pi. The EMBO journal *5*, 2637-2641.

14. Cross, R.A. (1988). What is 10S myosin for? Journal of muscle research and cell motility *9*, 108-110.

15. Trybus, K.M., and Lowey, S. (1984). Conformational states of smooth muscle myosin. Effects of light chain phosphorylation and ionic strength. The Journal of biological chemistry *259*, 8564-8571.

16. Sellers, J.R. (1991). Regulation of cytoplasmic and smooth muscle myosin. Current opinion in cell biology *3*, 98-104.

17. Seow, C.Y. (2005). Myosin filament assembly in an ever-changing myofilament lattice of smooth muscle. American journal of physiology. Cell physiology *289*, C1363-1368.

18. Milton, D.L., Schneck, A.N., Ziech, D.A., Ba, M., Facemyer, K.C., Halayko, A.J., Baker, J.E., Gerthoffer, W.T., and Cremo, C.R. (2011). Direct evidence for functional smooth muscle myosin II in the 10S self-inhibited monomeric conformation in airway smooth muscle cells. Proceedings of the National Academy of Sciences of the United States of America *108*, 1421-1426.

19. Xu, J.Q., Gillis, J.M., and Craig, R. (1997). Polymerization of myosin on activation of rat anococcygeus smooth muscle. Journal of muscle research and cell motility *18*, 381-393.

602   20.   Takahashi, T., Fukukawa, C., Naraoka, C., Katoh, T., and Yazawa, M. (1999). Conformations of
603         vertebrate striated muscle myosin monomers in equilibrium with filaments. Journal of biochemistry
604         *126*, 34-40.
605   21.   Ankrett, R.J., Rowe, A.J., Cross, R.A., Kendrick-Jones, J., and Bagshaw, C.R. (1991). A folded (10 S)
606         conformer of myosin from a striated muscle and its implications for regulation of ATPase activity. J
607         Mol Biol *217*, 323-335.
608   22.   Katoh, T., Konishi, K., and Yazawa, M. (1998). Skeletal muscle myosin monomer in equilibrium with
609         filaments forms a folded conformation. The Journal of biological chemistry *273*, 11436-11439.
610   23.   Woodhead, J.L., Zhao, F.Q., Craig, R., Egelman, E.H., Alamo, L., and Padron, R. (2005). Atomic model
611         of a myosin filament in the relaxed state. Nature *436*, 1195-1199.
612   24.   Stewart, M.A., Franks-Skiba, K., Chen, S., and Cooke, R. (2010). Myosin ATP turnover rate is a
613         mechanism involved in thermogenesis in resting skeletal muscle fibers. Proc Natl Acad Sci U S A
614         *107*, 430-435.
615   25.   Jung, H.S., Burgess, S.A., Billington, N., Colegrave, M., Patel, H., Chalovich, J.M., Chantler, P.D., and
616         Knight, P.J. (2008). Conservation of the regulated structure of folded myosin 2 in species separated
617         by at least 600 million years of independent evolution. Proc Natl Acad Sci U S A *105*, 6022-6026.
618   26.   Lee, K.H., Sulbaran, G., Yang, S., Mun, J.Y., Alamo, L., Pinto, A., Sato, O., Ikebe, M., Liu, X., Korn, E.D.,
619         et al. (2018). Interacting-heads motif has been conserved as a mechanism of myosin II inhibition
620         since before the origin of animals. Proc Natl Acad Sci U S A *115*, E1991-E2000.
621   27.   Pinto, A., Sanchez, F., Alamo, L., and Padron, R. (2012). The myosin interacting-heads motif is
622         present in the relaxed thick filament of the striated muscle of scorpion. Journal of structural biology
623         *180*, 469-478.
624   28.   Woodhead, J.L., Zhao, F.Q., and Craig, R. (2013). Structural basis of the relaxed state of a Ca2+-
625         regulated myosin filament and its evolutionary implications. Proc Natl Acad Sci U S A *110*, 8561-
626         8566.
627   29.   Zhao, F.Q., Craig, R., and Woodhead, J.L. (2009). Head-head interaction characterizes the relaxed
628         state of Limulus muscle myosin filaments. Journal of molecular biology *385*, 423-431.
629   30.   Zoghbi, M.E., Woodhead, J.L., Moss, R.L., and Craig, R. (2008). Three-dimensional structure of
630         vertebrate cardiac muscle myosin filaments. Proc Natl Acad Sci U S A *105*, 2386-2390.
631   31.   Cross, R.A., Jackson, A.P., Citi, S., Kendrick-Jones, J., and Bagshaw, C.R. (1988). Active site trapping
632         of nucleotide by smooth and non-muscle myosins. Journal of molecular biology *203*, 173-181.
633   32.   Liu, J., Wendt, T., Taylor, D., and Taylor, K. (2003). Refined model of the 10S conformation of
634         smooth muscle myosin by cryo-electron microscopy 3D image reconstruction. Journal of molecular
635         biology *329*, 963-972.
636   33.   Takizawa, Y., Binshtein, E., Erwin, A.L., Pyburn, T.M., Mittendorf, K.F., and Ohi, M.D. (2017). While
637         the revolution will not be crystallized, biochemistry reigns supreme. Protein Sci *26*, 69-81.
638   34.   Burgess, S.A., Walker, M.L., Thirumurugan, K., Trinick, J., and Knight, P.J. (2004). Use of negative
639         stain and single-particle image processing to explore dynamic properties of flexible
640         macromolecules. Journal of structural biology *147*, 247-258.
641   35.   Jung, H.S., Billington, N., Thirumurugan, K., Salzameda, B., Cremo, C.R., Chalovich, J.M., Chantler,
642         P.D., and Knight, P.J. (2011). Role of the tail in the regulated state of myosin 2. J Mol Biol *408*, 863-
643         878.
644   36.   Radermacher, M., Wagenknecht, T., Verschoor, A., and Frank, J. (1987). Three-dimensional
645         reconstruction from a single-exposure, random conical tilt series applied to the 50S ribosomal
646         subunit of Escherichia coli. Journal of microscopy *146*, 113-136.
647   37.   Fabiola, F., and Chapman, M.S. (2005). Fitting of high-resolution structures into electron
648         microscopy reconstruction images. Structure *13*, 389-400.

649  38.  Brown, J.H., Yang, Y., Reshetnikova, L., Gourinath, S., Suveges, D., Kardos, J., Hobor, F., Reutzel, R.,
650       Nyitray, L., and Cohen, C. (2008). An unstable head-rod junction may promote folding into the
651       compact off-state conformation of regulated myosins. Journal of molecular biology *375*, 1434-
652       1443.
653  39.  Spudich, J.A. (2015). The myosin mesa and a possible unifying hypothesis for the molecular basis of
654       human hypertrophic cardiomyopathy. Biochem Soc Trans *43*, 64-72.
655  40.  Scheres, S.H. (2012). RELION: implementation of a Bayesian approach to cryo-EM structure
656       determination. Journal of structural biology *180*, 519-530.
657  41.  Brito, R., Alamo, L., Lundberg, U., Guerrero, J.R., Pinto, A., Sulbaran, G., Gawinowicz, M.A., Craig, R.,
658       and Padron, R. (2011). A molecular model of phosphorylation-based activation and potentiation of
659       tarantula muscle thick filaments. Journal of molecular biology *414*, 44-61.
660  42.  Trybus, K.M., Freyzon, Y., Faust, L.Z., and Sweeney, H.L. (1997). Spare the rod, spoil the regulation:
661       necessity for a myosin rod. Proceedings of the National Academy of Sciences of the United States of
662       America *94*, 48-52.
663  43.  Olney, J.J., Sellers, J.R., and Cremo, C.R. (1996). Structure and function of the 10 S conformation of
664       smooth muscle myosin. The Journal of biological chemistry *271*, 20375-20384.
665  44.  Trybus, K.M., and Lowey, S. (1988). The regulatory light chain is required for folding of smooth
666       muscle myosin. The Journal of biological chemistry *263*, 16485-16492.
667  45.  Trybus, K.M., and Chatman, T.A. (1993). Chimeric regulatory light chains as probes of smooth
668       muscle myosin function. The Journal of biological chemistry *268*, 4412-4419.
669  46.  Espinoza-Fonseca, L.M., Kast, D., and Thomas, D.D. (2008). Thermodynamic and structural basis of
670       phosphorylation-induced disorder-to-order transition in the regulatory light chain of smooth
671       muscle myosin. Journal of the American Chemical Society *130*, 12208-12209.
672  47.  Ikebe, M., Ikebe, R., Kamisoyama, H., Reardon, S., Schwonek, J.P., Sanders, C.R., 2nd, and
673       Matsuura, M. (1994). Function of the NH2-terminal domain of the regulatory light chain on the
674       regulation of smooth muscle myosin. The Journal of biological chemistry *269*, 28173-28180.
675  48.  Taylor, K.A., Feig, M., Brooks, C.L., 3rd, Fagnant, P.M., Lowey, S., and Trybus, K.M. (2014). Role of
676       the essential light chain in the activation of smooth muscle myosin by regulatory light chain
677       phosphorylation. J Struct Biol *185*, 375-382.
678  49.  Nag, S., Trivedi, D.V., Sarkar, S.S., Adhikari, A.S., Sunitha, M.S., Sutton, S., Ruppel, K.M., and
679       Spudich, J.A. (2017). The myosin mesa and the basis of hypercontractility caused by hypertrophic
680       cardiomyopathy mutations. Nat Struct Mol Biol *24*, 525-533.
681  50.  Alamo, L., Wriggers, W., Pinto, A., Bartoli, F., Salazar, L., Zhao, F.Q., Craig, R., and Padron, R. (2008).
682       Three-dimensional reconstruction of tarantula myosin filaments suggests how phosphorylation
683       may regulate myosin activity. Journal of molecular biology *384*, 780-797.
684  51.  Alamo, L., Qi, D., Wriggers, W., Pinto, A., Zhu, J., Bilbao, A., Gillilan, R.E., Hu, S., and Padron, R.
685       (2016). Conserved Intramolecular Interactions Maintain Myosin Interacting-Heads Motifs
686       Explaining Tarantula Muscle Super-Relaxed State Structural Basis. J Mol Biol *428*, 1142-1164.
687  52.  Yount, R.G., Lawson, D., and Rayment, I. (1995). Is myosin a "back door" enzyme? Biophysical
688       journal *68*, 44S-47S; discussion 47S-49S.
689  53.  Persechini, A., and Hartshorne, D.J. (1981). Phosphorylation of smooth muscle myosin: evidence for
690       cooperativity between the myosin heads. Science *213*, 1383-1385.
691  54.  Persechini, A., and Hartshorne, D.J. (1983). Ordered phosphorylation of the two 20 000 molecular
692       weight light chains of smooth muscle myosin. Biochemistry *22*, 470-476.
693  55.  Trybus, K.M., and Lowey, S. (1985). Mechanism of smooth muscle myosin phosphorylation. The
694       Journal of biological chemistry *260*, 15988-15995.

695    56.    Wagner, P.D., Vu, N.D., and George, J.N. (1985). Random phosphorylation of the two heads of
696            thymus myosin and the independent stimulation of their actin-activated ATPases. The Journal of
697            biological chemistry *260*, 8084-8089.
698    57.    Ikebe, M., Hinkins, S., and Hartshorne, D.J. (1983). Correlation of intrinsic fluorescence and
699            conformation of smooth muscle myosin. The Journal of biological chemistry *258*, 14770-14773.
700    58.    Ikebe, M., Hinkins, S., and Hartshorne, D.J. (1983). Correlation of enzymatic properties and
701            conformation of smooth muscle myosin. Biochemistry *22*, 4580-4587.
702    59.    Houdusse, A., and Cohen, C. (1996). Structure of the regulatory domain of scallop myosin at 2 A
703            resolution: implications for regulation. Structure *4*, 21-32.
704    60.    Walcott, S., Fagnant, P.M., Trybus, K.M., and Warshaw, D.M. (2009). Smooth muscle heavy
705            meromyosin phosphorylated on one of its two heads supports force and motion. The Journal of
706            biological chemistry *284*, 18244-18251.
707    61.    Ikebe, M., and Hartshorne, D.J. (1985). Effects of Ca2+ on the conformation and enzymatic activity
708            of smooth muscle myosin. The Journal of biological chemistry *260*, 13146-13153.
709    62.    Burgess, S.A., Walker, M.L., Thirumurugan, K., Trinick, J., and Knight, P.J. (2004). Use of negative
710            stain and single-particle image processing to explore dynamic properties of flexible
711            macromolecules. J. Struct. Biol *147*, 247-258.
712    63.    Frank, J. (2006). Three-dimensional electron microscopy of macromolecular assemblies :
713            visualization of biological molecules in their native state, 2nd Edition, (Oxford ; New York: Oxford
714            University Press).
715    64.    Tang, G., Peng, L., Baldwin, P.R., Mann, D.S., Jiang, W., Rees, I., and Ludtke, S.J. (2007). EMAN2: an
716            extensible image processing suite for electron microscopy. J Struct Biol *157*, 38-46.
717    65.    Pettersen, E.F., Goddard, T.D., Huang, C.C., Couch, G.S., Greenblatt, D.M., Meng, E.C., and Ferrin,
718            T.E. (2004). UCSF Chimera--a visualization system for exploratory research and analysis. Journal of
719            computational chemistry *25*, 1605-1612.

720

721 **SUPPLEMENTARY FIGURES**

722

723



724
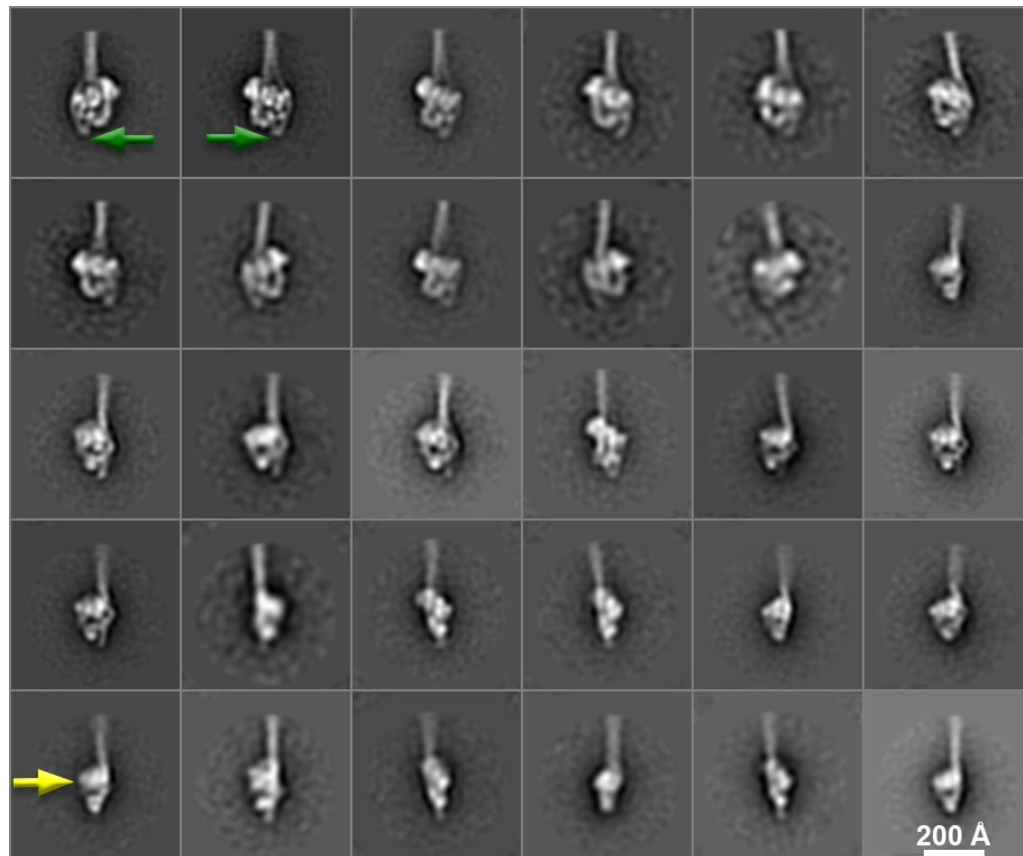
725 **Figure S1. 2D class averages of negatively stained 10S myosin molecules.** The appearances
726 of the different class averages indicate that the monomers tend to lie on the grid with the tail
727 parallel to the grid surface, but with different rotations about its long axis. Mirrored particles
728 indicated by green arrows represent face views of molecules lying face-up or face-down [2]; arrows
729 point specifically to hinge 2 (Fig. 1). Yellow arrow points to a side view.

730

731
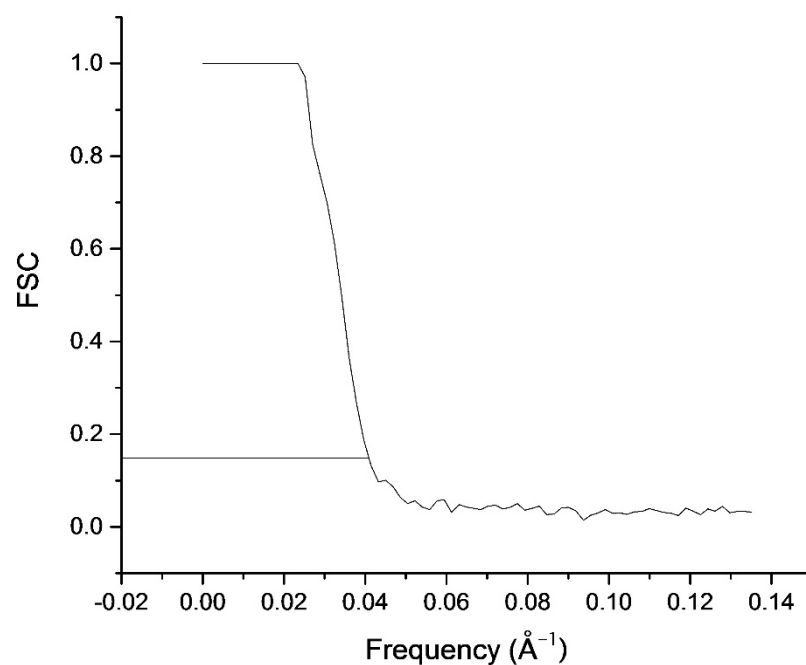
**Figure S2. Gold-standard Fourier shell correlation (FSC) curve to determine resolution.**

733

734



735
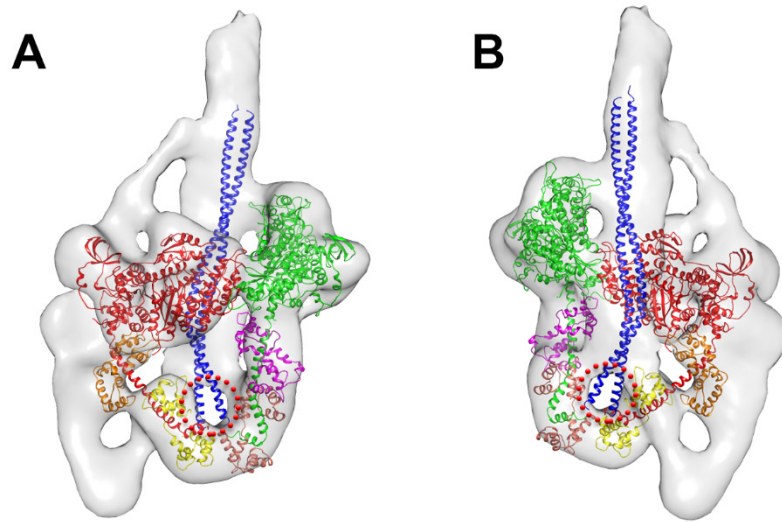
736 **Figure S3. Location of initial portion of subfragment 2.** Front and back views (A and B,
737 respectively) show the expected course of subfragment 2 (blue ribbon, based on ref. 21), starting
738 at the junction between the blocked and free head RLCs. The red dotted circle indicates an
739 absence of density in the reconstruction for the initial part of S2, probably due to mobility of this
740 part of the coiled-coil (see text and Fig. 3E).

741

742
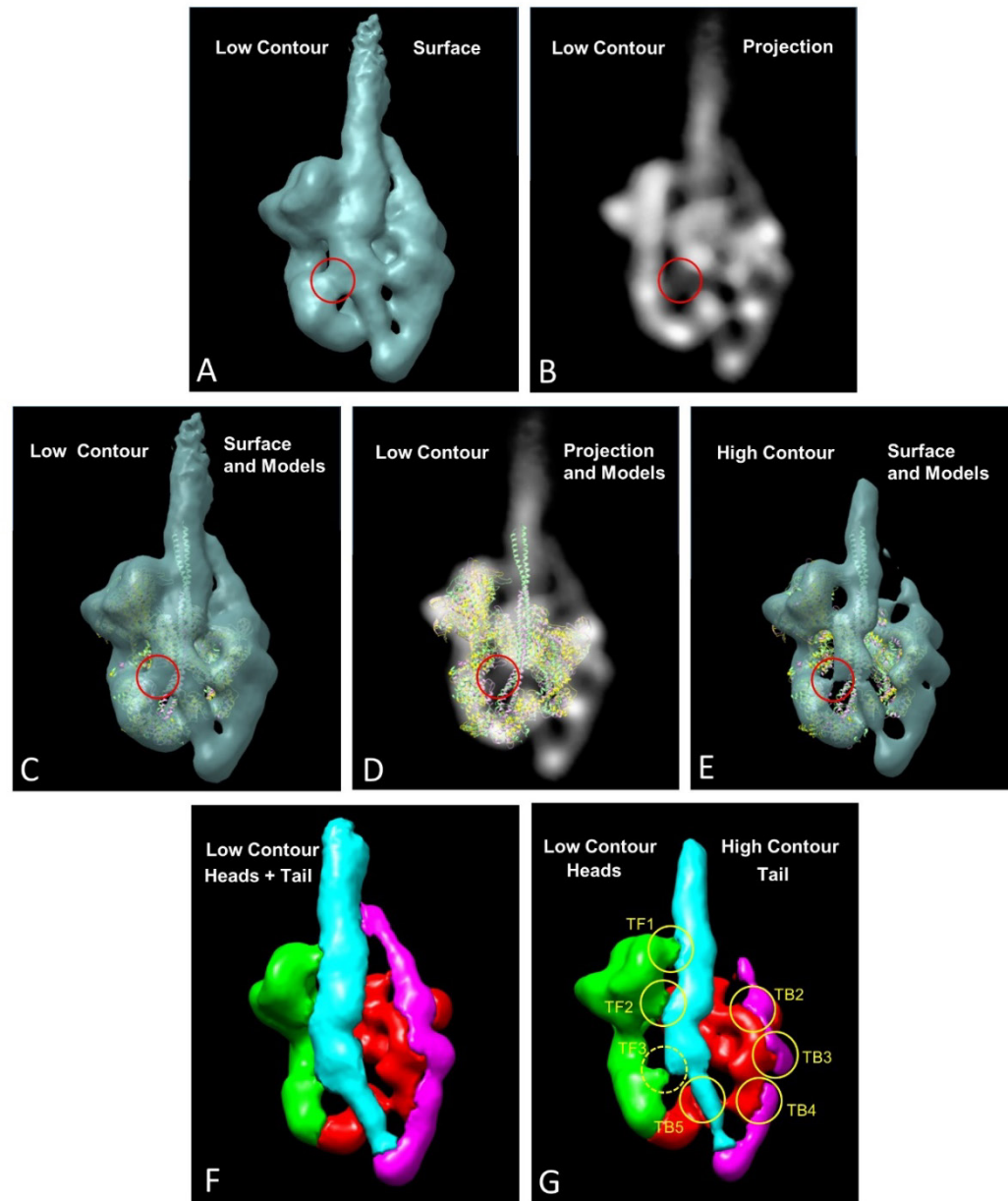
**Figure S4. Comparison of low and high contour cutoff reconstructions reveals the stronger and weaker parts of the density (rear views).** (A, B) Surface and projection (density) views. Apparent mass in low contour cutoff (circled interaction TF3 in (A)) is seen to have very little density in (B). (C-E) show TF3 in low (C) and high (E) contour cutoff surface views and in projection (D), with different variants of the IHM/S2 model fitted as in Fig. S3. Note disappearance of TF3 at high contour, and absence of protein density to fill the TF3 volume (circles). Note also difference in subfragment 2 density (bottom right of circle) between (C) and (E). Compare with Fig. S3. (F, G) With high contour cutoff, flexible regions of tail disappear (G), while contacts with the heads remain, suggesting that these are real interactions. The exception is TF3, which disappears.

752

27

753

754

755

756
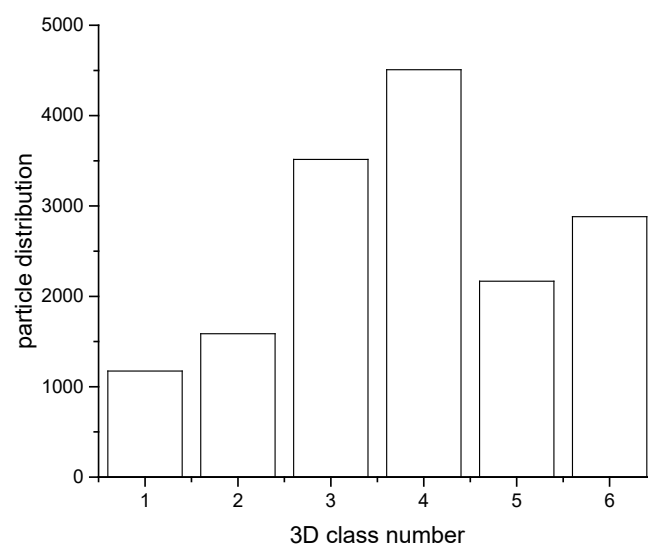
**Figure S5. Particle distribution of the 6 classes after 3D classification.** The corresponding 3D
reconstructions are shown in Fig. 6.

759

760



761
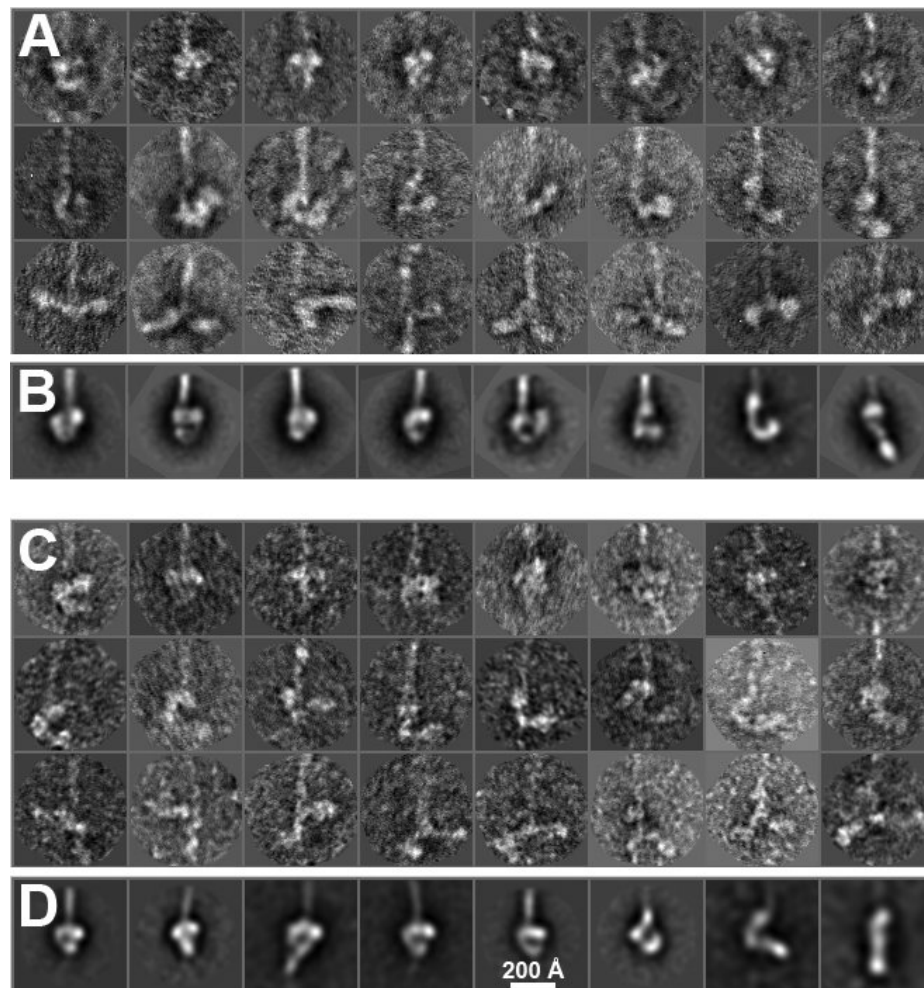
**Figure S6. Negatively stained insect indirect flight muscle (A,B) and *Dictyostelium* myosin II (C,D; unpublished data from [26]).** The top rows of (A) and (C) show molecules with a compact head arrangement in the IHM conformation. The second rows show dissociation of the free head from the blocked head, with the latter usually attached to subfragment 2. The free head exhibits gradual dissociation from the blocked head from left to right. The third rows show an open structure with no intramolecular interactions. (B) and (D) are 2D class averages of flight muscle and *Dictyostelium* myosin, respectively, computed to show the variability of head organization. The IHM is clearly demonstrated in the left images, while some averages on the right show the free head separated from the blocked head.

Interaction of segments 2 and 3 with the heads in smooth muscle 10S myosin considerably stabilizes the IHM. The above myosins, in which these interactions are weak or absent, serve to illustrate this point. Smooth muscle myosin clearly shows the second hinge point in 2D averages, a characteristic marker of the three-segment folded structure (green arrows, Fig. S1). The absence of this feature in many insect flight myosin molecules suggests that segments 2 and 3 are more weakly bound to the heads. Correspondingly, the free head tends to detach from the blocked head and the blocked head also becomes more mobile, as shown in (C) above. In *Dictyostelium*,

778     segment 3 continues past the two heads rather than making a second bend [26], and segment 2

779     does not appear to make interactions around the blocked head [26]. Correspondingly, free and

780     blocked heads again were frequently dissociated from each other and the tail.

781

782



783
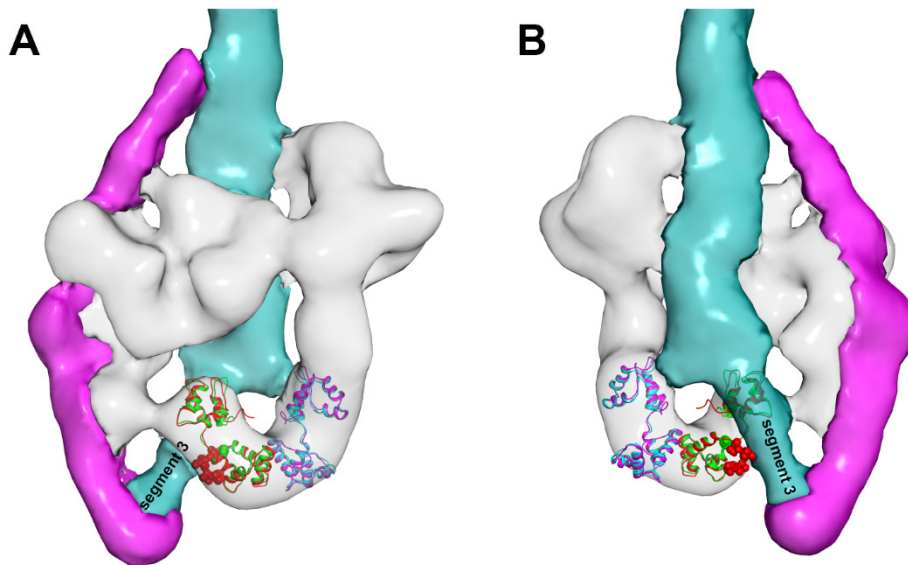
784 **Figure S7. The RLC N-terminal interacts with tail segment 3 in the 10S molecule.** The N-
785 terminal 24 residues of the smooth muscle RLC are absent in crystal structures due to mobility
786 (see text). To estimate their location, we docked the scallop RLC (3JTD; red, which has more
787 residues present) onto the smooth muscle RLC (green), so that the location of the additional
788 residues could be visualized. Residues 1-11 (red spheres, equivalent to residues 14-24 in smooth
789 muscle) suggest that the RLC N-terminal directly interacts with segment 3. A and B are front and
790 back views.

791 **SUPPLEMENTARY MOVIES**

792

793 **Movie 1. 3D reconstruction of 10S smooth muscle myosin rotated about its long axis (see**
794 **Fig. 3)**. Blocked head is red; free head, green; tail segments 1 and 3, cyan; segment 2, magenta.

795 **Movie 2. Atomic fitting of PDB-1I84 into the 3D reconstruction of 10S molecules (see Fig. 4).**
796 The densities attributed to the tail can be explicitly distinguished after atomic fitting. The path of the
797 tail wrapping around the heads can also be easily traced.
798
799 **Movie 3. Tail segment 3 contacts the RLC of the blocked head (see Fig. 5).** Segment 3 is seen
800 to closely approach Cys108 (cyan sphere) in the C-terminal lobe of the blocked head RLC.
801
802 **Movie 4. Tail segment 3 sterically block Ser19 on the blocked head (see Fig. 7).** Segment 2,
803 magenta; segment 3, cyan. Blocked head Ser19, red; free head Ser19, magenta. Note: The
804 blocked and free head RLCs of 1i84 are colored green and blue respectively. However, these
805 chains end at residue 25, owing to disorder of the N-terminus. To estimate the position of Ser19 in
806 each case, we superimposed the scallop RLC (red and magenta) on the smooth muscle RLC, and
807 have marked residue 19 in each case.